Materials Science Forum Vols. 369-372 (2001) pp. 277-286

The Influence of Water Vapor on the Corrosion of Chromia-Forming Steels

H. Asteman, K. Segerdahl, J.-E. Svensson and L.-G. Johansson

Department of Environmental Inorganic Chemistry, Chalmers University of Technology, SE-41296 Göteborg, Sweden

Keywords: 600°C, Active Corrosion, Evaporation, Fe-Cr Steel, Gas Velocity, Oxidation, Water Vapor

Abstract: The effect of gas velocity on the oxidation of three chromia-forming steels; X20 (11%Cr), 304L (18%Cr) and 310 (25%Cr) in O_2+40% H_2O at 600°C is reported. The samples are investigated by a number of surface analytical techniques including grazing angle XRD, SEM/EDX, and SAM. At low gas velocities a protective chromium-rich oxide forms on X20 and 310 while 304L shows partly protective behavior. With increasing gas velocity, the oxide tends to becomes more iron-rich and, consequently, less protective. The influence of gas velocity in O_2/H_2O environment is explained by the loss of chromium from the oxide through evaporation. The volatile species is suggested to be $CrO_2(OH)_2$. The different behavior shown by the three materials is explained in terms of the supply of chromium from the substrate to the oxide. Chromium depletion results in an increase in corrosion rate with gas velocity for all three materials and to "breakaway corrosion" in the case of X20.

1. INTRODUCTION

The effect of water vapor on the oxidation of Fe-Cr alloys is connected to the chemical composition of the oxide. Two different cases can be distinguished, on one hand the alloys that predominantly form iron oxides, on the other hand the alloys forming Cr-rich oxides. The latter class of materials, the so-called chromia formers, exhibits high resistance towards high temperature oxidation and corrosion because of the protection afforded by the Cr-rich oxide.

Chromia-forming alloys have been reported to be affected by water vapor in the sense that the critical amount of Cr to form protective Cr_2O_3 or $(Cr,Fe)_2O_3$ scales increases when water is present [1-3]. It has been suggested that H_2O reduces the stability of Cr_2O_3 or causes it to decompose [1]. Other workers [4-6] suggest that water vapor causes chromia to dissolve hydrogen ions, enhancing its ionic conductivity and resulting in a deterioration of the protective properties.

Some investigators suggest that the formation of volatile species such as $CrO_3(g)$, $CrO_2OH(g)$ or $CrO_2(OH)_2(g)$ [7-10] are responsible for the breakdown of chromia scales at temperatures above circa 1000°C. Graham and Davies [8] studied the flow-rate dependence of $CrO_3(g)$ evaporation from sintered Cr_2O_3 discs at 1200 °C in oxygen. They report that the addition of circa 2.5vol% of $H_2O(g)$ resulted in a 50% increase in the evaporation rate. It was suggested that this effect was caused by the formation of CrO_2OH (g).

Recent theoretical calculations [11-12], indicate that the hexavalent $CrO_2(OH)_2$ is the most stable vapor species in the $Cr/O_2/H_2O$ system rather than CrO_3 or the pentavalent CrO_2OH. Moreover, an evaluation of the thermodynamic properties of Cr-O-OH species by Ebbinghaus [9] indicates that

$CrO_2(OH)_2$ is the thermodynamically favored species in humid oxygen-rich atmospheres up to at least 1000°C.

In a previous investigation [13] we found that chromium is vaporized from 304L steel in O_2/H_2O environment already at 600°C. This was shown using a cooled probe where chromium oxide was collected. Chromium evaporation resulted in active corrosion that qualitatively followed Tedmon kinetics [7]. Using the thermodynamic data by Ebbinghaus [9], the equilibrium partial pressure of $CrO_2(OH)_2$ in the experiment was calculated to be about 1×10^{-6} atm.

If the corrosivity of water vapor is due to evaporation of $CrO_2(OH)_2$ (g), the rate of oxidation is expected to depend on pH_2O as well as on gas velocity. The effect of pH_2O is connected to thermodynamics as shown by the stoichiometry of the reaction:

$$1/2Cr_2O_3(s) + 3/4O_2(g) + H_2O \rightarrow CrO_2(OH)_2(g)$$

In contrast, the effect of flow rate is a kinetic effect that appears because the rate of evaporation is surface controlled. Volatile species diffuse from the surface, through the stagnant gas-phase layer separating the surface from the bulk gas, and are then carried away by the gas flow. As the gas velocity increases, the thickness of the diffusion layer diminishes, resulting in an increased evaporation rate.

The effect of pH_2O and flow-rate on the oxidation of 304L was demonstrated in an earlier paper [14]. In that paper, we showed that pH_2O and gas velocity both strongly affects the corrosion process. It was observed that high water concentrations (O_2 + 40%H_2O) and high gas velocities cause the 304L material to change from protective to non-protective behavior. A qualitative corrosion mechanism was proposed.

In order to test the validity of our previously proposed mechanism, the present study investigates the effect of flow rate on oxidation in O_2 + 40% H_2O at 600°C on three different chromia-forming steels: X20 (11%Cr), 304L (18%Cr) and 310 (25%Cr).

2. EXPERIMENTAL

X20, 304L and 310-coupons with the size 15/15/2mm (for steel composition, see Table 1) were exposed. The samples were ground on SiC-paper to 1000 mesh, polished with 1μm diamond paste and then cleaned in acetone and ethanol using ultrasonic agitation. The exposures were carried out in a horizontal furnace fitted with a 50 mm diameter SiO_2-glass tube. All exposures were isothermal, the temperature was kept at 600°, ±3°C.

The samples were mounted three at a time using a sample holder made from sintered alumina. The samples were positioned side by side and parallel to the direction of flow using slits in the sample holder. The distance between the samples was 12mm. This setup enables the samples to be exposed to the reaction gas with minimum contact with the sample holder and with optimal flow pattern. This way of mounting also minimizes the disturbance caused by the presence of multiple samples in the reactor.

A standard exposure time of 168 hours was selected. After each exposure the samples were cooled in dry air. Mass-changes were recorded on a five-decimal balance.

Exposures were made in a furnace system fitted with a humidifier producing a reaction gas consisting of O_2 + 40% H_2O (0.60 bar O_2 + 0.40 bar H_2O). Flow rates were 10, 200, 500, 1000,

2000 and 4000
10.0 cm/s, resp

X20	
304L	
310	

Table 1: Com
310 samples.

2.1 X-ray
Crystalline con
powder diffract
radiation was u
60°. The diffrac

2.2 Envir
Analytical scan
eXl EDX syste
analysis.

2.3. Scann
The Auger ana
beam voltage w
using a differen
rates were calil
collected raw-d
to evaluate peal
the signals fro
elements in oxi

3. RESU

3.1 Gravi
Before turning
represent the s
evaporation.

In addition to t
As expected, o
168 hours, all t
The mass-gain

Fig. 1 shows m
The insert shov
the three mate
suffers a mass
velocity increas

In the case of t
with the gas ve

2000 and 4000ml/min, corresponding to average net gas velocities of 0.025, 0.50, 1.24, 2.5, 5.0 and 10.0 cm/s, respectively.

	Cr (%)	Ni (%)	Mn(%)	Si(%)	Mo(%)	Fe(%)	nCr/nFe	Phase
X20	11.0	0.65	0.45	0.25	0.92	*Balance*	*0.14*	α/M
304L	18.5	10.2	1.41	0.55	0.49	*Balance*	0.29	γ
310	24.9	19.2	1.55	0.45	0.34	*Balance*	*0.50*	γ

Table 1: Composition (% by weight), molar ratio and phase composition of X20, 304L and 310 samples.

2.1 X-ray diffraction, (XRD)

Crystalline corrosion products were analyzed by X-ray diffraction (XRD) using a Siemens D5000 powder diffractometer equipped with grazing incidence beam attachment and a Göbel mirror. CuK_α radiation was used and the angle of incidence was 0.50°. The detector measures between $20° < 2\theta < 60°$. The diffraction peaks of the substrates were used as an internal standard.

2.2 Environmental Scanning Electron Microscopy, (ESEM/EDX)

Analytical scanning electron microscopy was carried out using a Electro-scan equipped with a Link eXl EDX system. The microscope was operated at 20 kV for secondary electron imaging and EDX analysis.

2.3. Scanning Auger electron microscopy, (SAM)

The Auger analyses were performed using a Scanning Auger Microprobe (PHI660). The electron beam voltage was 10 kV and the beam current was about 160 nA. The depth profiles were obtained using a differentially pumped ion gun (Ar^+) with acceleration voltages between 1.5 - 4 kV. The etch rates were calibrated on flat samples of Ta_2O_5 with a well-known oxide thickness of 1000 Å. The collected raw-data was refined by using MultiPak™ v.5.0 software. The software makes it possible to evaluate peak-shapes of differentiated Auger peaks. This feature was used to distinguish between the signals from oxidized and metallic iron and chromium, based on the chemical shifts of these elements in oxidized form.

3. RESULTS AND DISCUSSION

3.1 Gravimetry

Before turning to the gravimetric results it should be noted that the mass changes registered represent the sums of the mass gain due to oxide formation and the mass-loss connected to Cr-evaporation.

In addition to the water-vapor experiments, exposures were also carried out in dry O_2 for reference. As expected, oxidation in dry O_2 did not depend on flow. After oxidation in dry O_2 at 600 °C for 168 hours, all three materials had formed a thin adherent oxide film that was interference colored. The mass-gain in dry O_2 was 0.015, 0.023, 0.023mg/cm^2 for 310, 304L and X20, respectively.

Fig. 1 shows mass change after 168 hours in O_2+40%H_2O at 600 °C as a function of gas velocity. The insert shows the same data on a different scale. In O_2+40%H_2O environment the corrosion of the three materials is seen to be strongly dependent on gas velocity. The 310 (25%Cr) material suffers a mass loss at low flow velocities ($v \leq 2.5$cm/s), indicating active corrosion. As the flow velocity increased ($v \geq 5.0$cm/s), the material experience a mass gain.

In the case of the 304L (18%Cr) material, no mass loss was detected. Instead, mass gain increase with the gas velocity even at low flow rates ($v \leq 2.5$cm/s). It may be noted that the mass gain of

304L at high gas velocity is 5 to 6 times greater compared to exposure in dry O_2. This shows that high flow rates in O_2/H_2O environment cause a deterioration of the protective properties of the oxide formed on 304L.

At low gas velocities ($v \leq 2.5$cm/s), the X20 (11%Cr)-material suffer a small mass loss, signifying active corrosion. Similarly to the 310 (25%Cr) material, the mass loss recorded at low gas velocities change into a mass-gain at high gas velocities (see Fig.1). However, while the 310 material only experience a moderate increase in mass, X20 exhibited a mass gain that was about two orders of magnitude greater than in dry O_2. In effect, the X20 (11%Cr)-material exhibits excellent corrosion resistance in O_2/H_2O environment at low gas velocities but was transferred into a "breakaway corrosion" regime at high gas velocities.

To summarize the gravimetric results for the three Fe-Cr steels in O_2/H_2O environment at 600 °C, two of the materials (X20 and 310) formed highly protective oxide films at low gas velocities. In these cases a small weight loss was registered due to chromium evaporation. At high gas velocity breakaway corrosion was triggered on the X20 material. In addition, an "intermediate state" can be distinguished where the materials exhibited partly protective behavior. This can be seen in the case of 310 at high gas velocities and for 304L at low gas velocities. Below, we will proceed to show how these different types of corrosion behavior are related.

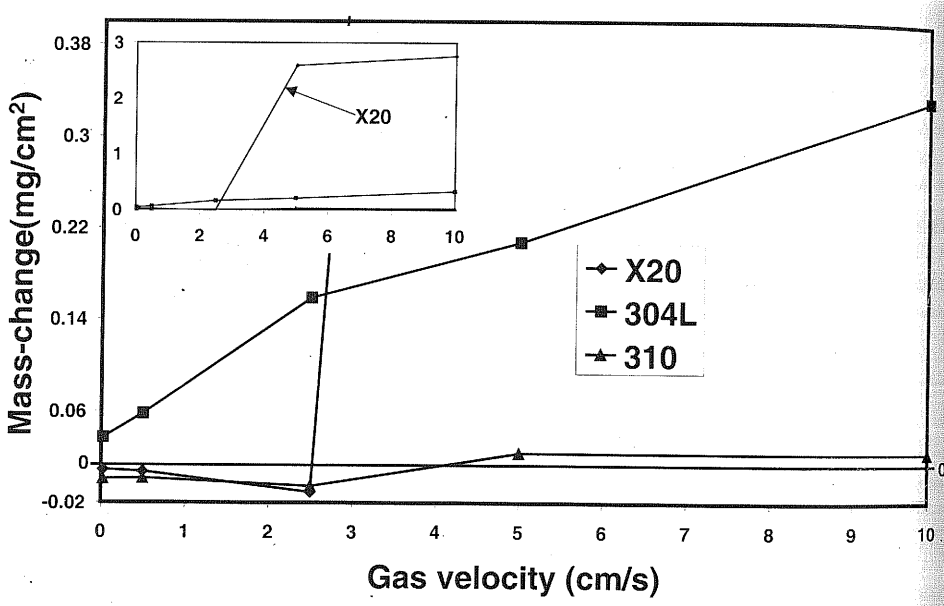

Figure 1: Mass change after exposure to O_2 + 40%H_2O for 168 hr at 600°C as a function of gas velocity. The insert shows the same data on a different mass scale. The scatter between the triplicate samples was about ± 10 % at small gas velocities and ± 5 % at high velocities.

3.2 Corrosion product characterization

Grazing incidence X-ray diffraction shows that the dominating corrosion product on all steels under all experimental conditions is an oxide iso-structural with corundum. In the case of the X20 samples oxidized at high flow-rates, XRD clearly indicates that α-Fe_2O_3 is the main corrosion product. However, in all other cases, the information obtained by XRD is not enough to pinpoint the nature of the oxide formed, as α-Fe_2O_3, Cr_2O_3 and the solid solutions α-$(Cr,Fe)_2O_3$ are all corundum type oxides with only minor differences in unit cell dimensions. For these oxides it is necessary to combine the XRD results with ESEM/EDX and SAM analysis to distinguish between the different possibilities.

Fig.2 shows ESEM images of the three materials after exposure in O_2 + 40%H_2O for 168hr at 600°C at different gas velocities. At low velocities ($v \leq 2.5$cm/s) the 310 material forms a thin uniform oxide film. SAM depth-profiling shows that the film is 30-40 nm thick and contains mainly Cr together with some Fe. An enrichment in chromium was found close to the oxide/steel interface while the outer part of the oxide is depleted in Cr. On the basis of the analysis by SAM and XRD it is concluded that the oxide consists of chromium-rich α-$(Cr,Fe)_2O_3$. As the flow rate increases there is a drastic change of morphology. Large (10-20 μm ∅) oxide islands form on the steel surface, separated by areas covered by a thin and smooth oxide film. In the thin oxide it is possible to discern a network pattern which is a projection of the grain boundaries in the steel substrate. SAM-depth profiling shows that the oxide islands are typically 6-10 μm thick and consist of two layers. The outer layer is made up of almost pure iron oxide while the inner layer has approximately equal amounts of iron and chromium. The thin film separating the oxide islands is identical in composition to the oxide film formed at low flow rate described above.

In contrast to the 310 material, 304L forms oxide islands even at low flow-rates. The oxide islands are similar to those formed on 310 at high gas velocities, the 10-20 μm ∅ and 6-15 μm thick islands being separated by a thin oxide film. This means that 304L does not form a thin, uniform oxide film regardless of flow rate when water vapor is present. The behavior of 304L and 310 also differs with respect to the thin oxide between the oxide islands. At low gas velocities both materials develop a thin (30-50 nm) oxide consisting of chromium-rich α-$(Cr,Fe)_2O_3$. As the gas velocity increases, the oxide on 304L grows in thickness to about 700nm while the Cr-concentration drops throughout the oxide, even at the oxide/steel interface. In the case of 310, there is no corresponding change in the thickness or composition of the "thin" oxide with the gas velocity. The increase in thickness in the thin oxide explains the high mass gain observed for 304L at high gas velocities.

We now turn to the results on the X20 (11% Cr) material. The mass-change curves in Fig. 1 show that, depending on the gas velocity, the material may exhibit protective behavior or suffer breakaway corrosion. These very different types of behavior are reflected in the composition and morphology of the corrosion products. At low gas velocity the material develops a protective 100nm thick chromium-rich α-$(Cr,Fe)_2O_3$ oxide film with no oxide islands present. The outer part of the film is depleted in Cr. Film morphology resembles that of 310 exposed to low flow velocities (see above). However, in contrast to the 310 material, the films on X20 do not exhibit a network pattern related to the grain structure in the metal.

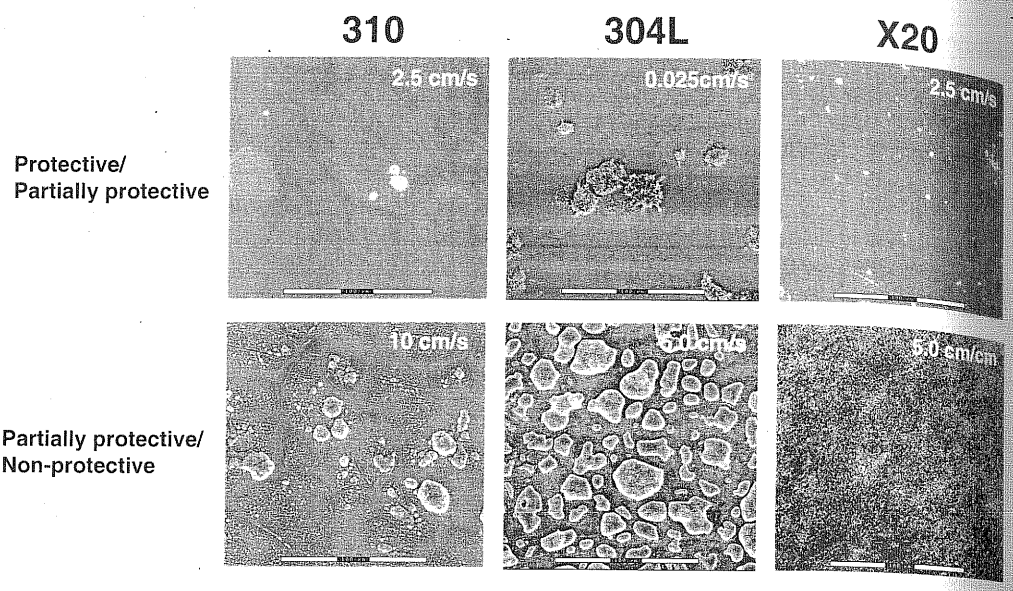

Figure 2: ESEM images of 310(25%Cr), 304L(18%Cr) and X20(11%Cr) steel coupons after exposure in O_2+40%H_2O for 168hr at 600°C at different gas velocities.

As the gas velocity is increased the material suffers breakaway behavior, the oxide growing in thickness to 15-20 μm. The ESEM images (see Fig. 2) shows little change in topography even though the oxide thickness has increased by 2 orders of magnitude. In contrast to the behavior of 304L and 310 at high flow rates, the thick oxide on X20 is uniform, covering all of the sample surface. The change in oxidation behavior is reflected in a compositional change in the oxide, from a chromium rich α-$(Cr,Fe)_2O_3$ to almost pure α-Fe_2O_3, as indicated by XRD.
This shows that "breakaway corrosion" occurs all over the X20 surface. In contrast, 304L and 310 experience breakaway corrosion only locally.

4 Discussion

We will now discuss the results in the light of our previously proposed mechanism [14]. It is necessary to briefly recall the main concepts of the mechanism (see Fig. 3).

In dry O_2 a protective oxide forms, consisting of a thin (30-100 nm) chromium rich α-$(Cr,Fe)_2O_3$. When water vapor is added, volatile chromium species in the form of oxy-hydroxides start to evaporate from the surface. As noted in the introduction, the evaporation rate depends on the equilibrium partial pressure of the volatile species and on gas velocity. The evaporation of chromium results in the depletion of the protective oxide with respect to chromium. At low evaporation rates the diffusion of chromium from the steel substrate is sufficiently rapid so that the chromium content in the oxide is not seriously lowered. The ability of the steel to supply the oxide with chromium depends on the chromium concentration and on the diffusion rate of chromium in the metal. A small grain size enhances the diffusivity of chromium because diffusion rates in the grain boundaries are high compared to the interior of a crystal. As the evaporation rate increases, the diffusion of chromium from the metal will eventually become insufficient in order to maintain a high chromium concentration in the oxide. When the chromium concentration in the oxide drops below a critical value at some point during the oxidation process, α-$(Cr,Fe)_2O_3$ changes from protective chromium-rich oxide to an oxide with properties that resemble those of the non-protective α-Fe_2O_3. Once an oxide with non-protective properties has formed, the oxidation rate increases dramatically.

This implies that the resistance of a chromia-forming steel towards the breakdown of the protective properties in O_2/H_2O environments is determined by : 1) The chromium concentration in the steel, 2) The bulk diffusivity of Cr in the steel and 3) The grain size of the metal.

It is apparent that the three materials are very different with respect to these properties. Fig. 3 illustrates schematically the effect of chromium evaporation on the oxidation behavior of the three materials. Turning first to the Cr-concentration (see Table 1), 310 exhibits the highest content while X20 is comparatively poor in Cr. Regarding bulk diffusivity, X20 is a tempered martensitic steel with either martensitic and/or α structure, while both 304L and 310 have austenitic structure. Metal diffusion in ferritic materials is much more rapid than in austenite so that bulk diffusivity of Cr is certainly highest in X20. There are also major differences in the grain structure of the three materials. The austenitic 304L and 310 have roughly equiaxial grains with an average diameter of 20-30 μm, while the martensitic X20 material has a more complex grain structure that depends on the thermal history of the sample. Generally, it is made up from former austenite grains, formed at high temperature during the steel production, which have been transformed to martensite during cooling. The lath-like martensitic grains are located inside the former gamma-grains in the form of flakes or discs with a thickness in the micron range. This leads to a high density of low-angle grain boundaries, which may act as rapid diffusion paths.

With respect to the supply of chromium to the oxide, the surface of the two austenitic steels can be subdivided into : 1) the areas in the vicinity of the grain-boundaries ; 2) the regions in the interior of the steel grains. Diffusivity in the grain boundaries is generally about 5 orders of magnitude greater compared to the undisturbed crystal [15]. This implies that the oxide formed in the vicinity of a grain boundary will be in contact with a substrate exhibiting a much greater diffusion rate of Cr than the oxide formed far from a grain boundary. The high abundance of grain-boundaries gives X20 much more homogenous diffusion properties, and all of the surface can be classified as equal to category 1) defined for the two austenitic steels.

The oxide formed on 304L/310 on type 2 areas with a low supply of Cr will become non-protective at lower evaporation rates than the oxide formed on areas with a high supply of Cr. This difference in behavior results in the uneven oxide shown in the ESEM images (see Fig. 2 and 3).

When the evaporation rate reaches a high enough level due to gas velocity, gas composition or temperature, both types of areas undergo breakaway corrosion but there is still a difference in oxide thickness (see Fig. 2 and 3). In the present study 304L exhibits a breakdown of protective properties close to the grain boundaries while 310 does not. The difference is presumably due to the lower Cr concentration in 304L. However, if the evaporation-rate is increased further because of higher gas speed or higher temperature, the 310 is expected to behave in a similar manner.

The behavior of X20 is completely different from that of the austenitic steels. Due to the rapid diffusion of Cr in the substrate and because of the high density of grain boundaries, all of the surface is supplied with chromium at a relatively high rate. This explains the material's excellent corrosion resistance at low gas velocities, even though the Cr-concentration is much lower than in 304L/310 (see table 2). As evaporation increases the oxide eventually becomes non-protective simultaneously on the whole surface, resulting in breakaway corrosion (see Fig. 3). This explains the abrupt change from active corrosion behavior to a massive mass gain at high gas speeds shown in Fig. 1. It should be noted that there is no indication of an intermediate state where parts of the surface are covered by a protective oxide while other parts are not, as in the case of 310 at high gas velocities.

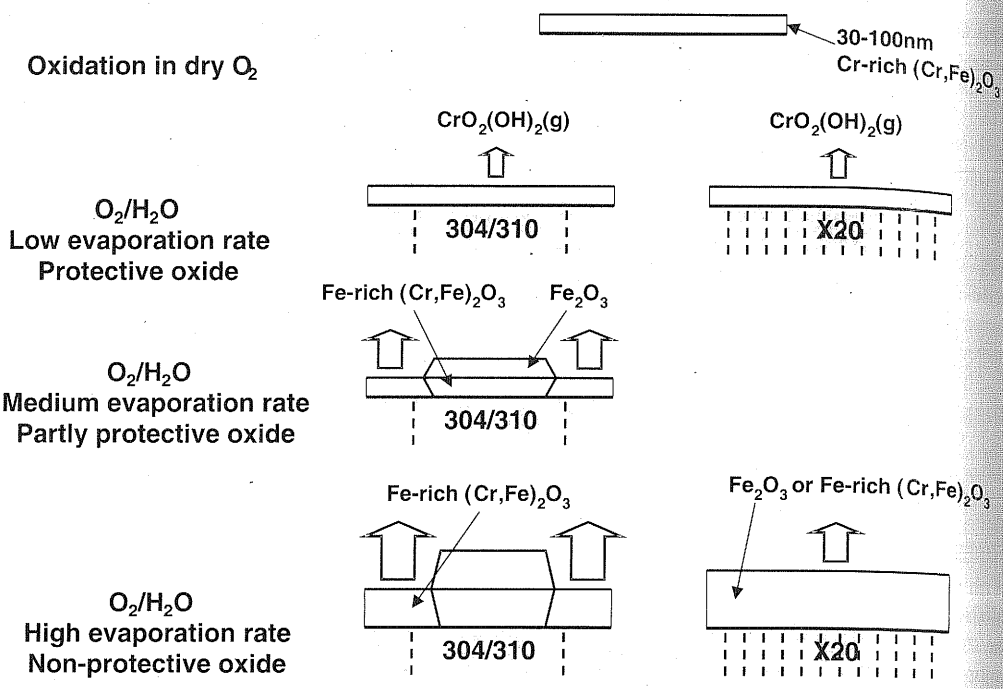

Figure 3: Schematic illustration of the oxidation of austenitic and ferritic chromium steels in O_2/H_2O environments. The illustration indicates the situation after 168 hours. The thick arrows indicate chromium evaporation.

5 CONCLUSIONS

The oxidation of X20(11%Cr), 304L(18%Cr) and 310(25%Cr) steels in O_2/H_2O environment is strongly affected by gas velocity. This is due to vaporization of chromium from the oxide in the form of chromium(VI) oxyhydroxide. At low gas velocities X20 and 310 show completely protective behavior. In both cases the excellent oxidation resistance is explained by the rapid supply of chromium to the oxide. In contrast, 304L does not form a completely protective oxide at low gas velocities. At high gas velocities, X20 exhibits breakaway corrosion while the oxide on 304L and 310 fails locally, as shown by the formation of iron-rich oxide islands (i.e. local breakaway corrosion). A qualitative mechanism is presented for the oxidation behavior of chromium steel in environments where chromium is lost by vaporization. The different behavior shown by the three materials is explained in terms of the supply of chromium from the substrate to the oxide. The resistance of chromia-forming steels towards high temperature corrosion in O_2/H_2O mixtures is enhanced by the following, substrate-related factors :

- High Cr concentration
- Fast diffusion in the steel bulk (ferrite rather than austenite)
- A high density of steel grain boundaries (small grain size)

The gas-phase related factors that tend to cause rapid corrosion in these environments are :

- High water vapor concentration
- High gas velocity
- High temperature

ACKNOWLEDGMENTS

This work was carried out within the Swedish High Temperature Corrosion Center (HTC).

REFERENCES

KOFSTAD P., "High-Temperature Corrosion", Elsevier Applied Science, London & New York, (1988), pp.382-385

KHANNA A.S., KOFSTAD P., Proceed. Intern. Conf. On Microscopy of Oxidation, London 1990, UK , (Inst. of Materials), pp. 113

ARMANET F., VEJUX A., BERANGER G., Behaviour of High-Temperature Alloys in Agressive Environments. London 1980, UK, (The Metals Society), pp.423, EUR 6814

FUJII C.T., MEUSSNER R. A., J. Electrochem. Soc. 111 (1964) 1215

HULTQUIST G., CHUAH G.K., TAN K.L., Corrosion Science 31 (1990) 149

NORBY T., J. de Physique IV 3 (1993) 99

TEDMON JR. C.S., J. Electrochem. Soc. 113 (1966) 766

GRAHAM H.C., DAVIES H.H., J. Am. Ceram. Soc. 54 (1971) 89

EBBINGHAUS B.B., Combustion and Flame 93 (1993) 119

STEARNS C.A., KOHL F.J., FRYBURG G.C., J. Electrochem. Soc. 121 (1974) 945

ESPELID Ø., BØRVE K.J., JENSEN V.R., J. Phys. Chem A 102 (1998) 10423

JOHNSON J.R.T., PANAS I., submitted to Inorg. Chem.

ASTEMAN H., SVENSSON J.-E., JOHANSSON L.-G., NORELL M., Oxid. Met. 52 (1999) 95

ASTEMAN H., SVENSSON J.-E., NORELL M., JOHANSSON L.-G., Oxid. Met. 54 (2000) 11

SUTTON A.P., BALLUFFI R.W., "Interfaces in Crystalline Materials", Oxford Science Publications, New York, (1995), chapter 8.